A Flexible Power Point Tracking Algorithm Based on Adaptive Lion Swarm Optimization for Photovoltaic System

Zongkui Xie
Yanshan University
Zhongqiang Wu (mewzq@163.com)
Yanshan University https://orcid.org/0000-0003-0650-9767

Research Article

Keywords: photovoltaic system, flexible power point tracking, lion swarm optimization, renewable energy

Posted Date: June 8th, 2022

DOI: https://doi.org/10.21203/rs.3.rs-881930/v1

A Flexible Power Point Tracking Algorithm Based on Adaptive Lion Swarm Optimization for Photovoltaic System

Zongkui Xie, Zhongqiang Wu*

（Key Lab of Industrial Computer Control Engineering of Hebei Province, Yanshan University, Qinhuangdao 066004,China）

Abstract

In order to weaken the adverse effects of PV grid connection on the power system and ensure the smooth operation of the system, a novel flexible power point tracking (FPPT) method based on adaptive lion swarm optimization (ALSO) is proposed in this paper. First, a reasonable objective function is established for the FPPT operating mode; the interval optimization method is used to distinguish the operating modes on both sides of the maximum power point (MPP). Secondly, ALSO is used to selectively optimize the operation of different intervals so as to achieve the FPPT control on the left or right side of the MPP. Through the simulation experiments on the PV grid-connected system, the validity and superiority of the ALSO-based method over the traditional FPPT algorithm in terms of dynamic and steady-state performance are verified under different operating conditions.

Keywords: photovoltaic system; flexible power point tracking; lion swarm optimization; renewable energy.

1. Introduction

Photovoltaic (PV) technology is a renewable energy power generation technology, which is an important method to mitigate the energy crisis and environmental pollution problems [1] [2]. Due to the continuous improvement of PV technology, the cost of PV panels is gradually decreasing; meanwhile, the installed PV capacity is increasing year by year. For example, the increased installed PV capacity in 2018 has reached 109GW, which is more than twice as much as the installed capacity in 2015 [3]. However, with the increasing number of grid-connected photovoltaic power plants (GCPVPP) and photovoltaic power generation, too much grid-connected power during the peak generation period may cause some adverse effects on the power system, such as overvoltage or overload. Flexible power point tracking (FPPT) is a new approach to address these issues in GCPVPP [4]-[7], which increasingly replaces the maximum power point tracking (MPPT) control strategy to provide more grid support functions.

According to recent references on FPPT, the existing FPPT algorithms fall into two main categories. The first type is the modification of the controller of the converter connected to the PV string to regulate the PV side power to its reference power [8]-[10]. This type of FPPT algorithms usually works by adjusting the reference voltage calculated by the MPPT in the “PV Voltage Control” block. The second type is the direct calculation of the reference voltage corresponding to its reference power [11]-[13]. In these algorithms, the voltage value corresponding to the reference

power is calculated using the FPPT algorithm, and the “PV Voltage Control” block is used to adjust the PV side voltage to its reference value given by the FPPT algorithm. Hossein Dehghani Tafti et al. [14] experimented with 11 algorithms of the two types. The experimental results show that the second class of algorithms outperforms the first class of algorithms in both dynamic and steady-state performance; meanwhile, these algorithms can switch MPPT or FPPT operating modes independently. Among the 11 algorithms, the general active power control method (GAPC) [15] works on the left or right side of the MPP in a dynamic environment better than the other 10 algorithms. In addition, it was also found that slight fluctuations in voltage can lead to relatively larger power oscillations due to the sensitivity of voltage to power variations on the right side of the MPP. As a result, the PV power of the above 11 algorithms operating on the right side of the MPP all deviated from their reference values by a relatively large margin. Therefore, how to improve the dynamic performance of the FPPT algorithm and how to improve the stability of GCPVPP remains a sticking point for the current researchers.

Among all the MPPT algorithms proposed in the past, there are many MPPT strategies based on artificial neural networks [16] or intelligence algorithms [17]-[20], in addition to the traditional increasing conductance (INC) [21] and perturb and observe method (P&O) [22]. However, there is very little literature applying intelligent algorithms to FPPT control. The reason is that there are two potential operating points (left or right side of the MPP) in FPPT mode. If an intelligent algorithm is applied directly to FPPT, the difference in the output each time will lead to severe oscillations in GCPVPP.

To address the above problems, a novel FPPT method based on adaptive lion swarm optimization (ALSO) is proposed in this paper. The inter-area optimization method is used to distinguish the operation modes on both sides of the MPP. The ALSO algorithm is used to selectively perform optimization on different regions to achieve FPPT control of the left and right sides of the MPP. The rest of the paper is structured as follows. The principle of FPPT control and main structure of GCPVPP are described in Section II. The details of ALSO algorithm are given in Section III. Section IV describes the ALSO-based FPPT algorithm in detail. Section V experimentally compares the performance of the method and the GAPC algorithm and provides a comprehensive comparison of the two algorithms. Finally, the concluding remarks and the innovation of this paper are given in Section VI.

2. FPPT and GCPVPP system

2.1 FPPT

During the peak generation period, excessive grid-connected electricity may cause some adverse effects on the power system, such as overvoltage or overload. To attenuate the adverse effects of grid-connected PV on the power

system, it is essential to introduce FPPT and MPPT control strategies to ensure the smooth operation of the system. Fig. 1 shows the operating points of the PV strings under different irradiance conditions.

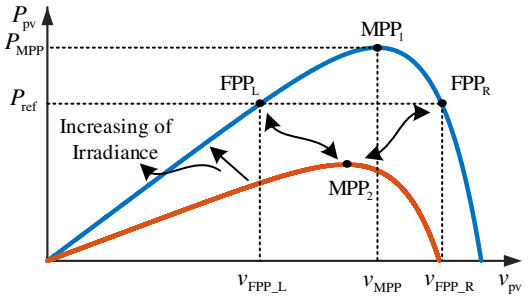

(a) The operating points of PV strings

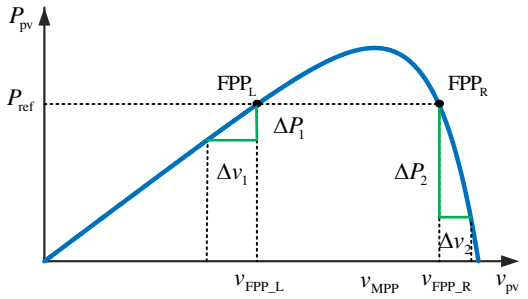

(b) Effect of the operating voltage change for output power

Fig.1 MPPT and FPPT in GCPVPP

As shown in Fig. 1 (a), when the maximum power of the PV string is less than the grid-connected reference power P_{ref}, the system always operates at MPP_2 controlled by the MPPT algorithm. As the irradiance increases, the available power gradually increases. If the maximum power is greater than P_{ref}, the operating point will move to the left or right side of the MPP, running at FPP_L or FPP_R. It is worth noting that, as shown in Fig. 1 (b), when the system is running at FPP_L, the changes in voltage will cause small power oscillations. Conversely, when the system is running at FPP_R, slight fluctuations in voltage will result in relatively larger power oscillations. As a result, most current FPPT algorithms makes the system more stable when operating at FPP_L than at FPP_R.

2.2 GCPVPP system

The GCPVPP system is divided into a single-stage system and a two-stage system. In the single-stage system, all control functions are implemented on the grid-connected inverter, which is directly connected to the PV strings. Although the single-stage system has the advantages of low power consumption and high efficiency, it cannot be guaranteed that the PV side voltage is greater than the peak grid voltage when voltage sag occurs. And in the case of only single-stage energy conversion, the two functions of MPPT and the grid-connected inverter cannot be well realized. The two-stage system is another structure of the GCPVPP system, as shown in Fig. 2, which can deal well

with the problems present in the single-stage system.

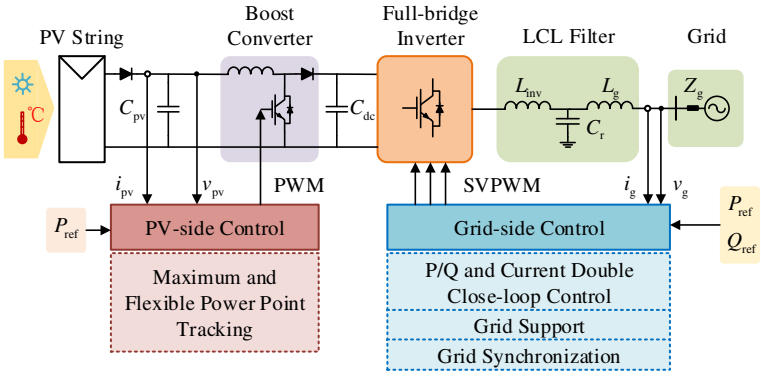

Fig.2 The structure of the two-stage GCPVPP

The system consists of a PV string, a boost converter, a full-bridge inverter, an LCL filter, a grid, a "PV side control" block, and a "grid-side control" block. In this structure, the PV string is connected to the full-bridge inverter via a boost converter, and the "PV-side control" block adjusts the duty cycle of the boost converter according to reference power (P_{ref}) to control the PV side voltage. The "grid side control" block uses P/Q, current dual closed-loop control and SVPWM for pulse modulation. Grid support section provides frequency support and fault ride-though capability. Grid synchronization can be achieved by phase-locked loops, which can calculate the grid voltage angle to synchronize the inverter current with the grid. As this paper mainly focuses on the FPPT of GCPVPP, the grid-connected aspect will not be expanded in detail, and the detailed structure of the system is shown in [23].

3. Adaptive lion swarm optimization

The main principle of lion swarm optimization (LSO) is described as follows [24] [25]. For all individuals in a population, the individual with the optimal fitness value is set as the "lion king", then some individuals are selected as "lionesses" and the remaining individuals are set as "cubs". In the optimization process, several lionesses hunt cooperatively. The cubs move around the adult lions. When the cubs grow up, they are expelled from the lion pack. After each search, the lion king reoccupies the position of the optimal fitness value.

Suppose there are N lions in the search space, the number of adult lions is N_{ad}, and the number of cubs is $N - N_{ad}$. The position of the ith lion is $x_i = x_{i1}, x_{i2}, \ldots, x_{iD}$, $1 \le i \le N$, and the adult lion with the optimal fitness value is set to "lion king"; the rest are "lionesses" and "cubs". The number of adult lions is

$$N_{ad} = \lceil N\beta \rceil \tag{1}$$

where β is the proportion of adult lions in the population, $\lceil \ \rceil$ means rounding up to an integer.

In the algorithm, different species of lions move differently in the optimization process. The lion king moves in a

small range to ensure its advantage and updates its position according to Eq. (2).

$$x_i^{k+1} = g^k \left(1 + \gamma \left\| p_i^k - g^k \right\| \right) \tag{2}$$

where γ is a normally distributed random variable, g^k is the best position of the *k*th generation, p_i^k is the best position of the *i*th individual of the *k*th generation, x_i^{k+1} is the updated position.

The lioness needs to cooperate with another lioness to hunt and update the position according to Eq. (3).

$$\begin{cases} x_i^{k+1} = \dfrac{\left(p_i^k + p_c^k\right)\left(1 + \alpha_f \gamma\right)}{2} \\ \alpha_f = step \cdot \exp\left(-\dfrac{30k}{T}\right)^{10} \end{cases} \tag{3}$$

where p_c^k is the position of another lioness randomly selected from the population; $step = 0.1 \cdot \left(ub - lb\right)$ represents the maximum step size of the cub; *ub* and *lb* are the upper and lower boundaries of the search space, respectively; *T* is the maximum number of iterations; *k* is the number of current iterations; α_f is the disturbance factor for updating the position of lionesses.

There are three ways to update the position of the cub, as shown in Eq. (4).

$$x_i^{k+1} = \begin{cases} \dfrac{\left(g^k + p_i^k\right)\left(1 + \alpha_c \gamma\right)}{2}, q \le \dfrac{1}{3} \\ \dfrac{\left(p_m^k + p_i^k\right)\left(1 + \alpha_c \gamma\right)}{2}, \dfrac{1}{3} < q \le \dfrac{2}{3} \\ \dfrac{\left(\overline{g}^k + p_i^k\right)\left(1 + \alpha_c \gamma\right)}{2}, \dfrac{2}{3} \le q \le 1 \\ \alpha_c = step \cdot \left(\dfrac{T - k}{T}\right) \end{cases} \tag{4}$$

where α_c is the disturbance factor for updating the position of the cubs; $\overline{g}^k = lb + ub - g^k$, $\overline{g}^k$ is the location where the cubs are driven out of the population; p_m^k is the position of the lioness followed by the lion cub. And *q* is a random number between 0 and 1. If $q < \frac{1}{3}$, the cubs hunt near the lion king g^k; if $\frac{1}{3} < q < \frac{2}{3}$, the cubs move around the lioness p_m^k; and if $q > \frac{2}{3}$, the cubs grow up.

In LSO, the behavior of lionesses is a “global search” mechanism and the behaviors of cubs are the “local search” mechanism and “avoid trapping in a locally optimal state” mechanism of the algorithm. Thus, the algorithm has a strong global search capability in the case of a large proportion of adult lions β; in contrast, the algorithm has a better ability to search finely and avoid trapping in the locally optimal solution. In order to further improve the performance of LSO

and increase the convergence speed, while taking into account the optimization accuracy, an adaptive lion swarm optimization is proposed. The improved proportion of adult lions is shown in Eq. (5).

$$\beta = \beta_{\max} - \left(\beta_{\max} - \beta_{\min}\right) \cdot k / T \tag{5}$$

where $\beta_{\max}$ and $\beta_{\min}$ are the upper and lower limits of β.

4. FPPT for GCPVPP based on ALSO

A GCPVPP system is modeled as shown in Fig. 2, and the "PV side control" block uses the ALSO algorithm to operate the FPPT. Considering that there are two potential operating points in the FPPT operation mode, if the intelligent algorithm is used directly for the FPPT operation, the output of the algorithm will be different, which will cause severe oscillations in the GCPVPP. For the above reasons, it is necessary to establish a reasonable objective function to ensure the smooth directional operations of the system.

4.1 The establishment of objective function

a) MPPT mode

When the available power of the PV strings is less than grid-connected reference power P_{ref}, the system always operates at MPP, so the objective function can be defined as:

$$f_1(v) = \max P(v) = \max(v \cdot I(v)) \tag{6}$$

where $P = v \cdot I$ is the PV side power, $v \in [0, v_{\text{oc}}]$, and v_{oc} is the open circuit voltage.

b) FPPT mode

When the available power of the PV strings is greater than grid-connected reference power P_{ref}, the system will operate at FPP_{L} or FPP_{R} (as shown in Fig. 1), and $f_1(v)$ is no longer applicable to the FPPT mode. Therefore, the new objective function is designed as follows.

$$\begin{aligned} f_2(v) &= \max\left(P_{\text{ref}} - \left|P - P_{\text{ref}}\right|\right) \\ &= \max\left(P_{\text{ref}} - \left|vI(v) - P_{\text{ref}}\right|\right) \end{aligned} \tag{7}$$

where P_{ref} is the reference power, $v \in [0, v_{\text{MPP}}]$ or $v \in [v_{\text{MPP}}, v_{\text{oc}}]$, v_{MPP} is the voltage of the MPP. The function curve of $f_2(v)$ is shown in Fig.3.

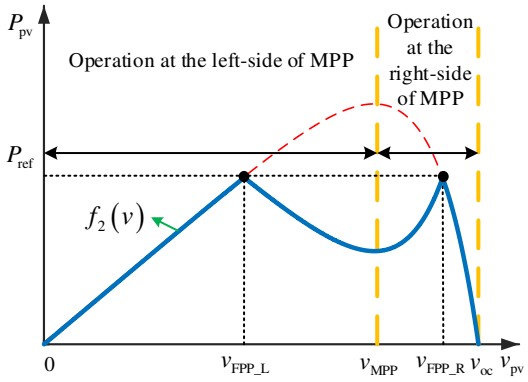

Fig.3 The function curve of the objective function in FPPT mode

As shown in Fig. 3, the design principle of f_2 is that the part greater than P_{ref} is folded down and $[0, v_{oc}]$ is divided into two parts, $v \in [0, v_{MPP}]$ and $v \in [v_{MPP}, v_{oc}]$, which are the different intervals with operating at the left or right side of MPP.

4.2 FPPT based on ALSO

Fig.4 describes the schematic of the FPPT algorithm based on ALSO.

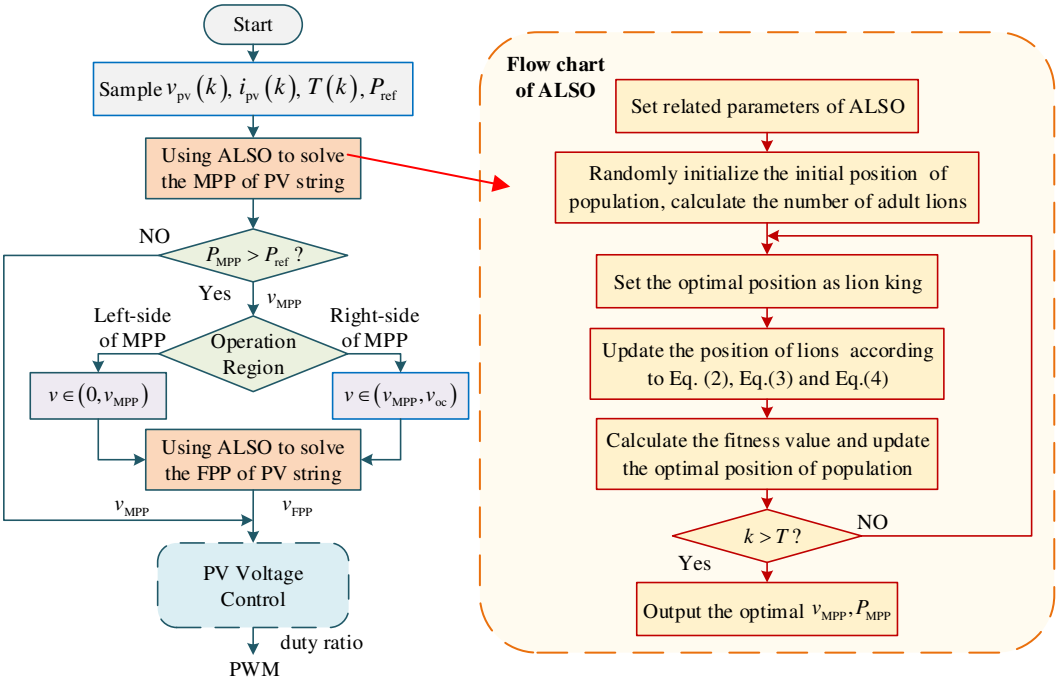

Fig.4 The schematic of the FPPT algorithm based on ALSO

As shown in Fig. 2 and 4, the workflow of the system is as follows. First, the P_{ref}, PV side current and PV side voltage are entered into the "PV side control" block, and the maximum value of $f_1(v)$ (available power) and its corresponding voltage (v_{MPP}) are calculated using ALSO. If the available power is less than P_{ref}, v_{MPP} will be considered as the reference voltage for controlling the operation of the system at that point. If the available power

is greater than P_{ref}, then ALSO will be used to optimize the output voltage of $f_2(v)$ over the range of $v \in [0, v_{MPP}]$ (operation at left side of MPP) or $v \in [v_{MPP}, v_{oc}]$ (operation at left side of MPP), outputting the optimal voltage (v_{FPP}), and v_{FPP} will be considered as the reference voltage for controlling the operation of the system at that point.

5. Simulation results

In order to evaluate the effectiveness and accuracy of the proposed FPPT algorithm, the GCPVPP system is modeled and simulated using Simulink, as shown in Fig. 2, and the parameters of the system are listed in Table 1. The performance of the algorithm is compared with the GAPC reported in [15], and the parameter values of the two algorithms are shown in Table 2.

Table 1 Parameters of the GCPVPP system

Parameter	Symbol	Values
PV maximum power	P_{MPP}	502kW
PV maximum power voltage	V_{MPP}	502V
PV maximum power current	I_{MPP}	1000A
PV capacitor	C_{pv}	3mF
dc-dc boost converter inductor	L_{boost}	10mH
dc-dc switching frequency	$f_{sw\text{-}boost}$	10kHz
Grid-connected inverter filter	L_{inv}	3mH
Inverter switching frequency	$f_{sw\text{-}inv}$	10kHz

Table 2 Parameters of ALSO and GAPC

Algorithm	Parameter
ALSO	N=20, T=10, $\beta_{max}=0.8$, $\beta_{min}=0.05$
GAPC	Left: V_{step}=3.5, T_{step}=0.001, k_1=0.001, k_2=0.085
	Right: V_{step}=1.5, T_{step}=0.001, k_1=0.006, k_2=0.05

In order to accurately evaluate the response performance of the system, the cumulative tracking error (*TE*) is introduced to measure the steady-state and dynamic performance of the two algorithms in FPPT mode, which is defined as follows:

$$\begin{cases} TE = \sqrt{TE_{ss}^{\ 2} + TE_{tr}^{\ 2}} \\ TE_{ss} = \dfrac{\int \left| P_{pv} - P_{fpp} \right|}{\int \left| P_{pv} \right|} \times 100, \text{steady state} \\ TE_{tr} = \dfrac{\int \left| P_{pv} - P_{fpp} \right|}{\int \left| P_{pv} \right|} \times 100, \text{transient} \end{cases} \tag{8}$$

where TE_{ss} is the steady-state tracking error and TE_{tr} is the transient tracking error.

The simulations were performed under two conditions, a rapid change in irradiance and a change in reference power. In addition, both algorithms were simulated in the left and right operating regions.

5.1 Fast change of the irradiance

In this section, the irradiance varies with time, as shown in Fig. 5. Three different reference values are used for the simulation of the two algorithms, i.e., 80% (Case 1, P_{ref}=400kw), 50% (Case 2, P_{ref}=250kw), and 20% (Case 3, P_{ref}=100kw) of the MPP of the PV strings, respectively.

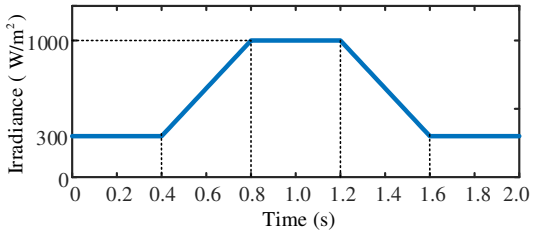

Fig.5 Solar irradiance curve

The response performances of the two algorithms is shown in Fig. 6 and 7. In Fig. 6 and 7, P_{avai} is the available power value; P_{ref} is the reference power value; P_{pv_1}, P_{pv_2} and P_{pv_3} are the PV side power of Case1, Case2 and Case3, respectively, and *Irr* is the irradiance value.

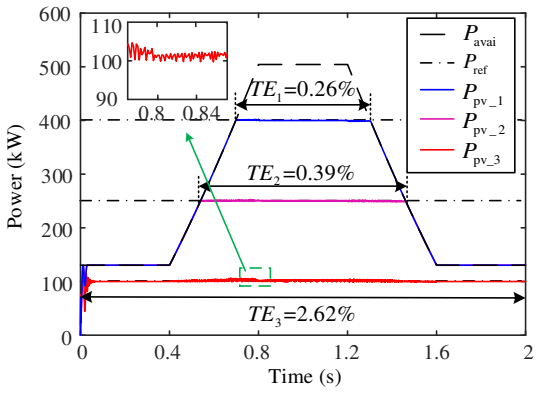

(a1) PV power of ALSO

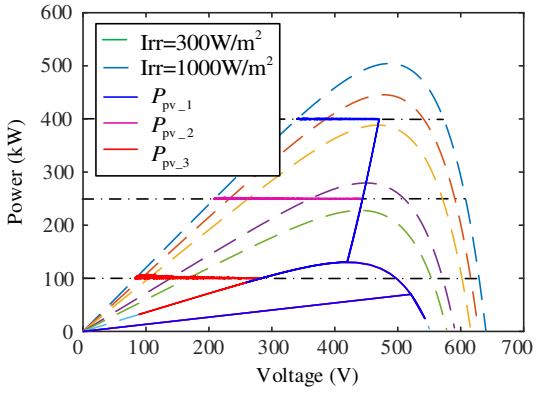

(a2) Operating point of ALSO

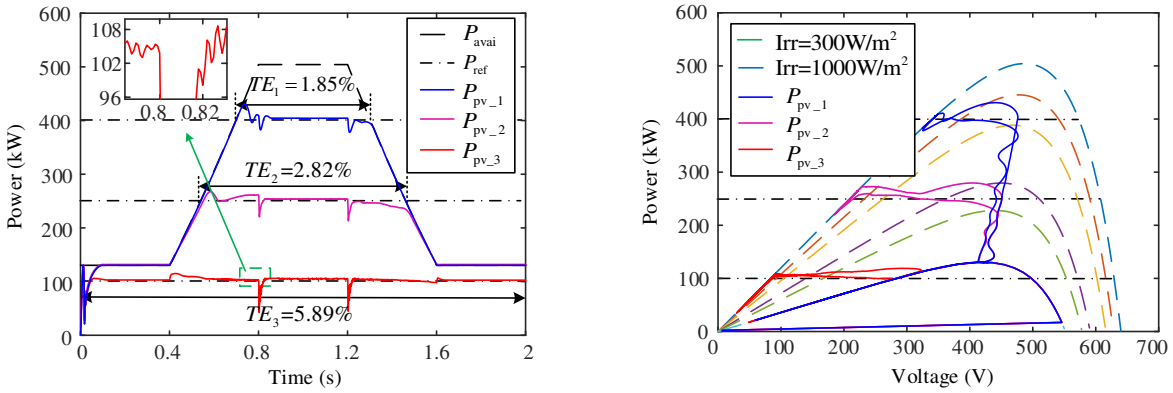

(b_1) PV power of GAPC (b_2) Operating point of GAPC

Fig.6 The response performances of the two algorithms under fast changes of irradiance with operating at the left-side of MPP

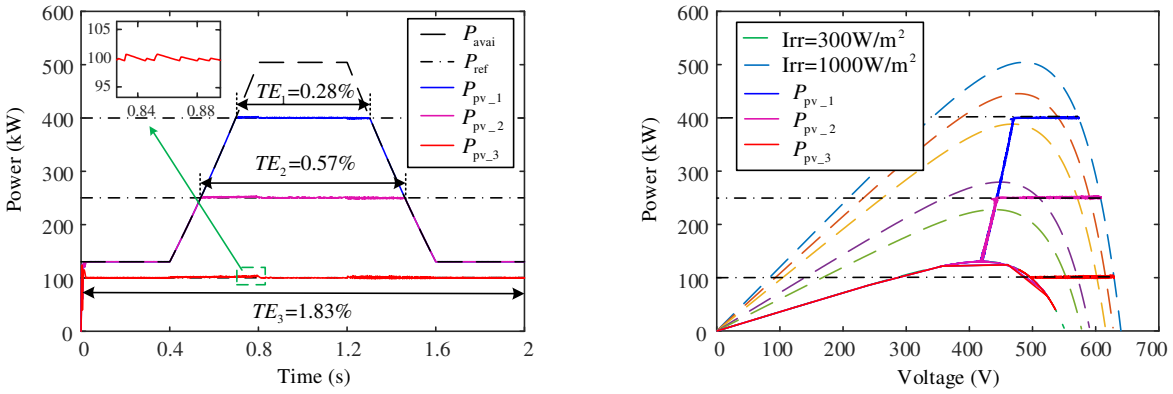

(a_1) PV power of ALSO (a_2) Operating point of ALSO

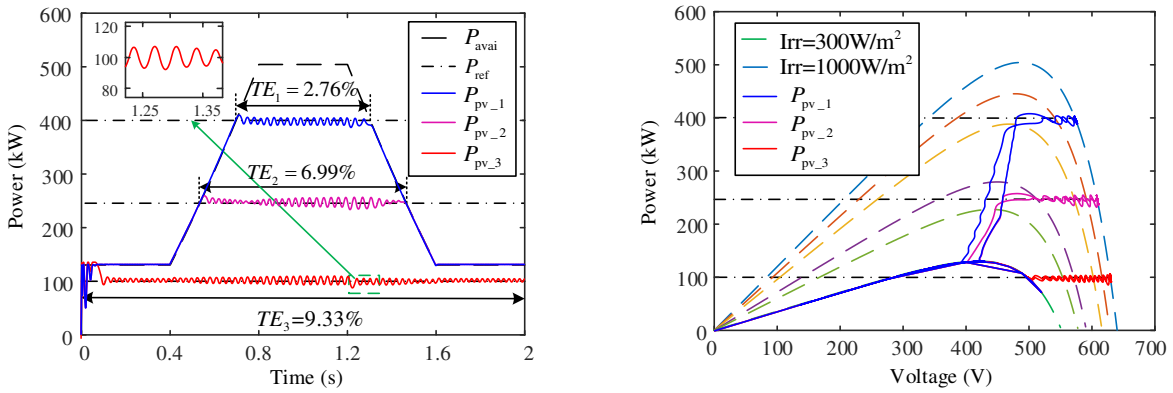

(b_1) PV power of GAPC (b_2) Operating point of GAPC

Fig.7 The response performances of the two algorithms under fast changes of irradiance with operating at the right-side of MPP

The response performance of the two algorithms when running on the left side of the MPP is shown in Fig. 6. It can be seen from Fig. 6 (a_1) that ALSO can adjust the PV side power to P_{ref} under three cases when running on the left side of MPP. Both the dynamic and steady-state processes operate smoothly. The tracking error is small in all cases, TE_1=0.26%, TE_2=0.39% and TE_3=2.62%, respectively. Fig. 6 (a_2) shows the operating points of the PV strings in the three cases, and the ALSO can approach the P_{ref} steadily and accurately. Fig. 6 (b_1) and (b_2) show the performance of

the GAPC in the three cases when running on the left side of the MPP. Although the steady-state process of GAPC is similar to that of ALSO, the dynamic process of GAPC has some oscillations in all cases. And its tracking error is larger than ALSO with TE_1=1.85%, TE_2=2.82% and TE_3=5.89%, respectively.

The response performance of the two algorithms when operating on the right side of MPP is shown in Fig. 7. The system with the ALSO algorithm still maintains smooth dynamic and steady-state processes in all three cases with tracking errors that are not much different from those operating on the left side of the MPP. For GAPC, on the other hand, the PV side power deviates significantly from its references values in both steady-state and dynamic operation; the error is relatively large in all cases.

5.2 Varying reference power

In this section, the irradiance is set to a constant (Irr=800W/m^2) and the reference power varies with time, as shown in Fig. 8.

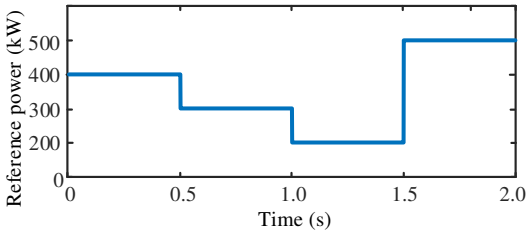

Fig.8 Reference power curve

Fig. 9 and 10 show the performance of the two algorithms when running on the left or right side of the MPP.

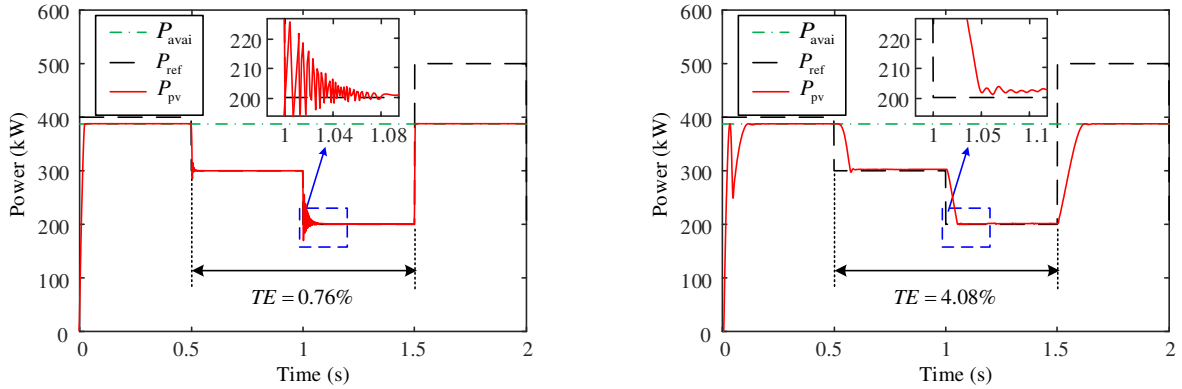

(a) PV power of ALSO

(b) PV power of GAPC

Fig.9 The response performances of the two algorithms under fast changes of reference power with operating at the left-side of MPP

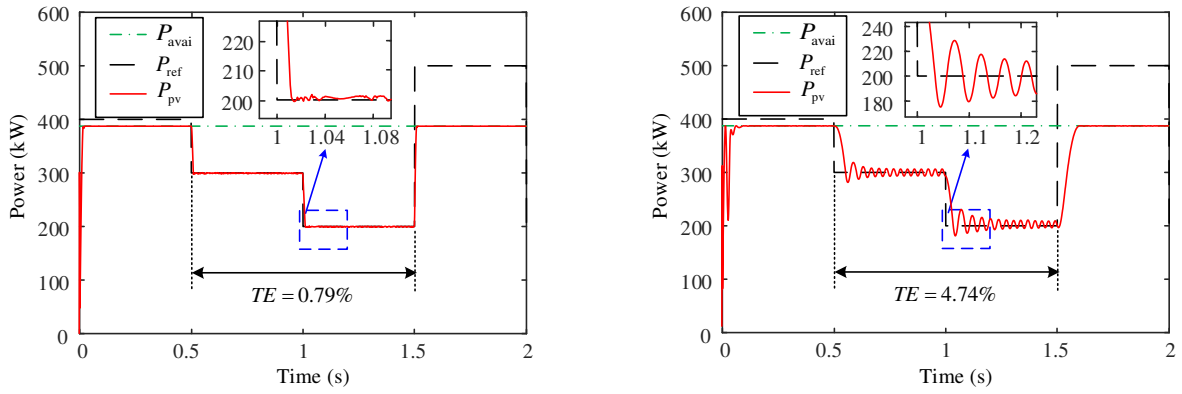

(a) PV power of ALSO

(b) PV power of GAPC

Fig.10 The response performances of the two algorithms under fast changes of reference power with operating at the right-side of MPP

It can be seen from the graphs that P_{avai} is smaller than P_{ref} in the interval from t=0s to t=0.5s and from t=1.5s to t=2s, during which the system works on MPP. Both algorithms perform well for MPPT, while the ALSO algorithm has a significantly shorter tracking time than GAPC. In the interval from t=0.5s to t=1.5s, P_{ref} decreases and is smaller than P_{avai}, as shown in Fig. 9 (a) and Fig. 10 (a), and the tracking error of ALSO is exceptionally small during steady state. At t=1s, the P_{ref} changes from 300kW to 200kW, and accordingly, the PV side power drops to 200kW. The output power of ALSO quickly tracks to its reference value after a short oscillation, and the tracking error is TE=0.76% for operation at left side of MPP and TE=0.79% for operation at right-side of MPP, respectively. The steady-state error of the GAPC algorithm when operating on the left side of MPP is also small, while working on the right side of the MPP, there is a relatively large deviation from its reference value, as shown in Fig. 9 (b) and Fig. 10 (b).

5.3 Comparison of ALSO and GAPC

In order to visually compare and analyze the performance of the two algorithms, the tracking errors were calculated for all cases in 5.1 and 5.2 above and are listed in Table 3.

Table.3 Comparison of tracking error indices of two algorithms

Algorithm	Operation region	Fast change of irradiance									Varying reference power (%)		
		Case1 (%)			Case2 (%)			Case3 (%)					
		TE_{ss}	TE_{tr}	TE	TE_{ss}	TE_{tr}	TE	TE_{ss}	TE_{tr}	TE	TE_{ss}	TE_{tr}	TE
ALSO	Left	**0.02**	**0.26**	**0.26**	**0.22**	**0.32**	**0.39**	**1.76**	**1.96**	**2.62**	**0.76**	-	**0.76**
	Right	**0.14**	**0.24**	**0.28**	**0.27**	**0.50**	**0.57**	**0.85**	**1.63**	**1.83**	**0.79**	-	**0.79**
GAPC	Left	1.19	1.4	1.85	2.03	1.96	2.82	4.61	3.67	5.89	4.08	-	4.08
	Right	1.25	2.47	2.76	5.24	4.62	6.99	6.58	6.62	9.33	4.74	-	4.74

In Table 3, it should be noted that the TE_{ss}, TE_{tr} and TE of the ALSO algorithm are much smaller than those of the GAPC algorithm in all above cases. Compared to the GAPC algorithm, the tracking error of the ALSO algorithm is at most 40% of the GAPC algorithm (Case3, working on the left side of the MPP) and at least 8% of the GAPC algorithm (Case2, working on the right side of the MPP). Second, the smaller the reference power, the larger the tracking error when the system is operating at rapidly changing irradiance. Obviously, the TE of the ALSO algorithm differs little when operating on the left and right sides of the MPP.

In summary, the method based on the ALSO algorithm can autonomously switch the operating modes of MPPT and FPPT in a dynamic environment. In addition, the method has good stability when running on both sides of the MPP, and the tracking error is much smaller than the GAPC algorithm, which verifies the superiority of the proposed method.

6. Conclusion

In order to ensure the smooth operation of GCPVPP, this paper proposes a novel FPPT method based on ALSO. The main contributions and innovations can be summarized in the following three aspects.

1) The adaptive proportion factor is introduced in the LSO algorithm. The number of adult lions accounts for a larger proportion in the early stage of the iteration and a smaller proportion in the final stage of the iteration, which can effectively improve the convergence speed and optimization accuracy of the algorithm.

2) Since there are two potential operating points in the FPPT mode, if the intelligent algorithm is used directly for FPPT, the algorithm will produce different outputs each time, which will cause severe oscillations in the GCPVPP. For this reason, a new objective function has been established for the FPPT mode, which uses interval optimization to distinguish the operating modes on both sides of the MPP. Therefore, the ALSO algorithm can be used to selectively calculate the reference voltage of the MPP or the FPP at different intervals to achieve FPPT control on either the left or the right side of the MPP.

3) The simulation results under both conditions show that, compared with GAPC, the ALSO-based FPPT algorithm can ensure the smooth operation of the system on both sides of MPP in a dynamic environment, which compensates for the fact that the traditional FPPT algorithm cannot operate smoothly on the right side of MPP. In particular, the tracking error is reduced by 60% to 92% compared with GAPC, which proves the effectiveness and superiority of the proposed FPPT method for GCPVCC.

Conflict of Interest

Authors declare that they have no conflict of interest.

Ethical approval

This article does not contain any studies with human participants or animals performed by any of the authors.

Acknowledgement

This project was supported by the Natural Science Foundation of Hebei Province under Grant F2020203014.

Data availability

Data sharing not applicable to this article as no datasets were generated or analysed during the current study.

References

[1] Xie ZK, Wu ZQ. Maximum power point tracking algorithm of PV system based on irradiance estimation and multi-Kernel extreme learning machine 2021; 44: 101090.

[2] Hultmann Ayala HV, Coelho LDS, Mariani VC, Askarzadeh A. An improved free search differential evolution algorithm: a case study on parameters identification of one diode equivalent circuit of a solar cell module. Energy 2015; 93:1515-1522.

[3] REN21, "Renewables 2018: Global status report (GRS)," 2018. [Online]. Available: http://www.ren21.net/

[4] Gevorgian V, ONeill B. Advanced grid-friendly controls demonstration project for utility-scale PV power plants. National Renewable Energy Laboratory report, NREL no. NREL/TP-5D00-65368, USA, Jan. 2016. [Online].

[5] Tafti HD, Maswood AI, Konstantinou G, Pou J, Blaabjerg F. A general constant power generation algorithm for photovoltaic systems. IEEE Transactions on Power Electronics 2018; 33: 4088-4101.

[6] V. Gevorgian, Highly Accurate Method for Real-Time Active Power Reserve Estimation for Utility-Scale Photovoltaic Power Plants. USA: National Renew. Energy Lab., Feb. 2019.

[7] Chamana M, Chowdhury BH, Jahanbakhsh F. Distributed control of voltage regulating devices in the presence of high PV penetration to mitigate ramp-rate issues. IEEE Transactions Smart Grid 2018; 9: 1086-1095.

[8] Mirhosseini M, Pou J, Agelidis VG. Single- and two-stage inverter-based grid-connected photovoltaic power plants with ride-through capability under grid faults. IEEE Transactions on Sustainable Energy 2015; 6: 1150-1159.

[9] Tafti HD, Maswood AI, Konstantinou G, Pou J, Kandasamy K, Lim Z, Ooi GHP. Low-voltage ride-thorough capability of photovoltaic grid-connected neutral-point-clamped inverters with active/reactive power injection. IET Renewable Power Generation 2017; 11: 1182-1190.

[10] Tafti HD, Maswood AI, Konstantinou G, Pou J, Acuna P. Active/reactive power control of photovoltaic grid-tied inverters with peak current limitation and zero active power oscillation during unbalanced voltage sags. IET Power Electronics 2018; 11: 1066-1073.

[11] Tafti HD, Maswood AI, Konstantinou G, Pou J, Blaabjerg F. A general constant power generation algorithm for photovoltaic

systems. IEEE Transactions on Power Electronics 2018; 33: 4088-4101.

[12] Sangwongwanich A, Yang Y, Blaabjerg F. A sensorless power reserve control strategy for two-stage grid-connected PV systems. IEEE Transactions on Power Electronics 2017; 32: 8559-8569.

[13] Sangwongwanich A, Yang Y, Blaabjerg F, Wang H. Benchmarking of constant power generation strategies for single-phase grid-connected photovoltaic systems. IEEE Transactions on Industry Applications 2018; 54: 447-457.

[14] Tafti HD, Konstantinou G, Townsend CD, Farivar GG, Sangwongwanich A, Yang Y, Pou J, Blaabjerg F. Extended Functionalities of Photovoltaic Systems with Flexible Power Point Tracking: Recent Advances. IEEE Transactions on power electronics 2020; 35: 9342-9356.

[15] Tafti HD, Sangwongwanich A, Yang Y, Konstantinou G, Pou J, Blaabjerg F. A general algorithm for flexible active power control of photovoltaic systems. 2018 IEEE Applied Power Electronics Conference and Exposition (APEC), 1115-1121.

[16] Lin HJ, Zhou BX, Ran Y, Zhan CJ, Yang CY. Research on maximum power point tracking of photovoltaic system based on genetic algorithm BP neural network algorithm. Electrical Measurement and Instrumentation 2015; 52: 35-40.

[17] Kumar N, Hussain I, Singh B, Panigrahi BK. Single Sensor-Based MPPT of Partially Shaded PV System for Battery Charging by Using Cauchy and Gaussian Sine Cosine Optimization. IEEE Transactions on Energy Conversion 2017; 32: 983-992.

[18] Kumar N, Hussain I, Singh B, Panigrahi BK. Normal Harmonic Search Algorithm-Based MPPT for Solar PV System and Integrated With Grid Using Reduced Sensor Approach and PNKLMS Algorithm. IEEE Transactions on Industry Applications 2018; 54: 6343-6352.

[19] Wu ZQ, Yu DQ. Application of improved bat algorithm for solar PV maximum power point tracking under partially shaded condition. Applied Soft Computing 2018; 62: 101-109.

[20] Wu ZQ, Yu DQ, Kang XH. Application of improved chicken swarm optimization for MPPT in photovoltaic system. Optimal Control Applications and Methods 2018; 39: 1029-1042.

[21] Tey KS, Mekhilef S. Modified incremental conductance MPPT algorithm to mitigate inaccurate responses under fast-changing solar irradiation level. Solar Energy 2014; 101: 333-342.

[22] Mohamed AI, Sayed MA, Mohamed EEM. Modified efficient perturb and observe maximum power point tracking technique for gridtied PV system. International Journal of Electrical Power &Energy Systems 2018; 99: 192-202.

[23] Fu WW, Zeng CB, Zhang JQ, Liu YY. Improvement of grid transient stability by optimizing power regulation of photovoltaic power generation. Chinese Journal of Power Sources 2017; 41: 786-789.

[24] Liu SJ, Yang Y, Zhou YQ. A Swarm Intelligence Algorithm - Lion Swarm Optimization. Pattern Recognition and Artificial Intelligence 2018; 31: 431-441.

[25] Wu ZQ, Xie ZK, Liu CY. An improved lion swarm optimization for parameters identification of photovoltaic cell models.

Transactions of the Institute of Measurement and Control 2020; 42(6): 1191-1203